Organic & Biomolecular Chemistry

ROYAL SOCIETY OF CHEMISTRY

PAPER

View Article Online
View Journal

Cite this: DOI: 10.1039/d0ob01347a

Guest-induced supramolecular chirality transfer in [2]pseudorotaxanes: experimental and computational study†

Hui-Juan Wang,‡[a] Hao-Yang Zhang,‡[a] Heng-Yi Zhang,*[a] Guoxing Liu,[b] Xianyin Dai,[a] Huang Wu[a] and Yu Liu*[a]

Received 1st July 2020,
Accepted 14th September 2020

DOI: 10.1039/d0ob01347a

rsc.li/obc

To reveal the factors governing the chirality transfer from a chiral unimolecule to a supramolecular assembly, we constructed a series of [2]pseudorotaxanes through the intermolecular noncovalent interaction of a pair of chiral binaphthalene crown ethers with achiral secondary ammonium salts with different chromophores, and found that the binaphthalene groups can induce new circular dichroism (CD) signals only in the [2]pseudorotaxane structures between the host crown ethers and the guest molecule with the anthryl group. Density functional theory (DFT) and time-dependent density functional theory (TD-DFT) calculations show that the generation of the new CD signal is mainly due to the intermolecular chiral induction between the anthryl group in the guest and the naphthalene groups in the host.

Introduction

Supramolecular chirality[1] arises from chirality transfer, chirality amplification and asymmetry breakage between chiral or achiral components,[2,3] which has sparked scientists' curiosity for the development of asymmetric catalysis,[4–7] chiroptical advanced materials,[8–11] biomimetics,[12,13] chiral recognition[14–16] and sensors.[17,18] The rapid development of supramolecular chemistry and molecular self-assembly provides versatile strategies to produce supramolecular chirality, which usually include three aspects. That is, there are (a) chiral molecules,[19] (b) combination of chiral and achiral molecules,[20–22] or (c) aggregation of exclusively achiral molecules[23] in supramolecular systems. In the meantime, chirality transfer starting from single molecular chirality to a supramolecular chiral system has drawn increasing attention.[24] In order to produce effective chirality transfer, it is important to have strong interaction between the chiral molecule and achiral molecule.[1] It is an ingenious strategy to construct a chirality transfer system by combining chirality and host–guest chemistry. Many supramolecular chiral systems have been reported, but most of them are based on the self-assembly of a single component or co-assembly of two or more components which have similar structures.[2,25] There are a few reports of guest-induced supramolecular chirality. For example, Hayashita *et al.* developed supramolecular chirality induced by 15C5-Azo-dpa inside the chiral cavity of γ-cyclodextrin due to the recognition of ions by a guest molecule.[26] Bhalla *et al.* reported pyrazine derivatives with L-alanine groups as chiral building blocks and the system's supramolecular chirality could be controlled by guests.[27] Recently, we constructed some photo-controlled chirality transfer systems based on pseudorotaxanes. One is a snowflake-like supramolecular clockwise-helical assembly whose chirality can be controlled by the photo-isomerization of azobenzene,[20] and another is a photochromic [3]pseudorotaxane whose induced circular dichroism (ICD) signals can be tuned by the photo-oxidation of anthracene.[28] Nevertheless, to the best of our knowledge, no structure-based systematic approach has been employed in the attempts to understand and control the supramolecular chirality transfer based on multicomponent supramolecular systems. In this context, it is essential to systematically investigate the chirality transfer behavior of related host–guest chemistry comparatively with different π-systems.

In the present study, we constructed a series of [2]pseudorotaxanes *via* the noncovalent interaction between a pair of binaphthalene crown ethers (*S*)-**1**/(*R*)-**1** and four secondary ammonium salts **2–5** with different aromatic cores, ranging from phenyl, naphthyl, and anthryl to pyrenyl (Scheme 1), and systematically investigated their binding mode and the photophysical behavior by NMR, UV, fluorescence and circular

[a]College of Chemistry, State Key Laboratory of Elemento-Organic Chemistry, Nankai University, Tianjin 300071, P. R. China. E-mail: hyzhang@nankai.edu.cn, yuliu@nankai.edu.cn
[b]College of Chemistry and Chemical Engineering, Henan University of Technology, Zhengzhou 450001, P. R. China

†Electronic supplementary information (ESI) available: Experimental and characterization. See DOI: 10.1039/d0ob01347a

‡These authors contributed equally to this work.

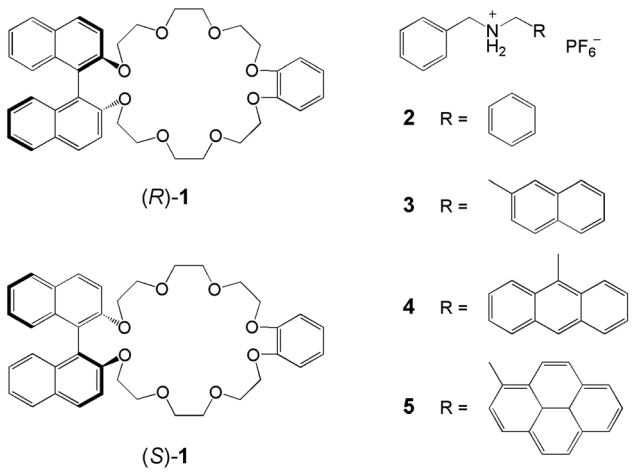

Scheme 1 Chemical structures of two host crown ethers (*R*)-**1** and (*S*)-**1**, and four guest secondary ammonium molecules **2**–**5**.

dichroism (CD) spectroscopy, and density functional theory (DFT) and time-dependent density functional theory (TD-DFT) calculations. It is of particular interest to us to elucidate the origin of the supramolecular chirality transfer from chiral binaphthalene crown ethers to [2]pseudorotaxanes. These studies will aid our understanding of the chirality transfer in supramolecular systems and may further contribute to the prediction of macroscopic chirality of a wide variety of supramolecular aggregation.

Results and discussion

The formation of [2]pseudorotaxanes through the interaction of binaphthalene crown ethers with secondary ammonium salts can be conveniently monitored by ^{1}H NMR spectroscopy. As can been seen from Fig. 1, upon the equivalent mixing of (*S*)-**1** and **4** in dichloromethane, the proton signals of **4** and (*S*)-**1** both exhibit significant changes in the spectrum. These observations suggest that the secondary ammonium cation moiety of **4** threads into the crown ether ring of (*S*)-**1**.[29,30] A similar phenomenon has also been observed in the ^{1}H NMR spectra of the equivalent mixture of (*S*)-**1**/(*R*)-**1** and **2**–**5** (Fig. S8, S9, S10†), which indicates the formation of [2]pseudorotaxanes between hosts and guests.

CD spectroscopy

CD spectroscopy is a versatile and widely used chiroptical technique which possesses the advantage of directly differentiating supramolecular chirality without the assistance of other chiral substances.[31] The CD spectra of hosts (*S*)-**1** (red line) and (*R*)-**1** (black line) are shown in Fig. S11.† Strong Cotton effects between 238 and 342 nm (λ_{max} = 248 nm, λ_{min} = 284 nm split from $\lambda_{\theta=0}$ = 269 nm) are presented. According to the previous reports, the CD signals could be due to the exciton coupling of ^1B_b transitions of the two naphthalenes,[32] while the positive Cotton effects at 247 nm ($\Delta\varepsilon$ = 115 L mol^{-1} cm^{-1}) are the classical signals of the 1,1′-binaphthyl chromophore.[33–35] In addition, negatively intense CD signals were observed at 284 nm ($\Delta\varepsilon$ = −29 L mol^{-1} cm^{-1}) and 321 nm ($\Delta\varepsilon$ = −17 L mol^{-1} cm^{-1}). The CD spectrum of (*R*)-**1** is shown in Fig. S11† (black line). As expected, the CD signals of (*R*)-**1** were completely opposite to those of (*S*)-**1** which means a couple of enantiomers were obtained.

The [2]pseudorotaxanes constructed by hosts ((*R*)-**1** and (*S*)-**1**) and guests (**2**–**5**) were respectively investigated by CD spectroscopy. From the CD spectrum of **4** ⊂ (*S*)-**1** (Fig. 2a), we can see that the Cotton effect value of (*S*)-**1** at 248 nm was dramatically weakened to zero and two small peaks (split from $\lambda_{\theta=0}$ = 253 nm) appeared at the original wavelength region. It still showed slightly stronger Cotton effects between 271 nm and 322 nm (λ_{max} = 283 nm, $\Delta\varepsilon$ = −36 L mol^{-1} cm^{-1}) compared to (*S*)-**1**. Significantly, new negative triple peaks were displayed at 358 nm, 374 nm and 395 nm after two crossovers at 242 nm and 350 nm. Obviously, the triple peaks are characteristic

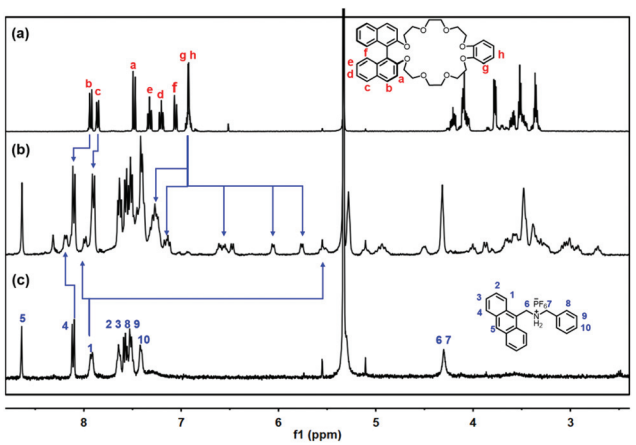

Fig. 1 Partial ^{1}H NMR spectra (400 MHz, 298 K, 1.0 × 10^{-3} M) recorded in CD_2Cl_2 for (a) (*S*)-**1**, (b) an equimolar mixture of (*S*)-**1** and **4** and (c) **4**.

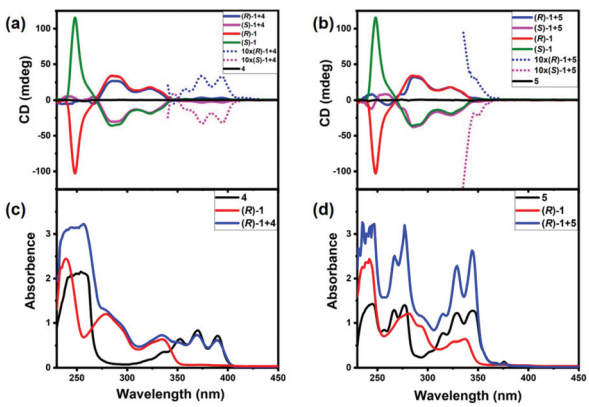

Fig. 2 Circular dichroism spectra of (a) **4**, (*R*)-**1**, **4** ⊂ (*R*)-**1**, (*S*)-**1** and **4** ⊂ (*S*)-**1** and (b) **5**, (*R*)-**1**, **5** ⊂ (*R*)-**1**, (*S*)-**1** and **5** ⊂ (*S*)-**1** in CH_2Cl_2 : CH_3CN = 20 : 1, and UV-vis absorbance spectra of (c) **4**, (*R*)-**1** and **4** ⊂ (*R*)-**1** and (d) **5**, (*R*)-**1** and **5** ⊂ (*R*)-**1** in CH_2Cl_2 : CH_3CN = 20 : 1; [(*R*)-**1**] = [(*S*)-**1**] = [**4**] = [**5**] = 10^{-4} M; path length: 10 mm.

absorption peaks of the anthracene chromophore.[36] The new Cotton effects are believed to arise from the intermolecular chirality induction between anthracene and naphthalene chromophores, while the CD spectrum of **4** ⊂ (*R*)-**1** showed new opposite positive triple peaks, which means the new Cotton effects were determined by the configuration of the host. We further verified that the new CD signals were caused by the intermolecular chirality transfer from the naphthalene chromophores in the host to the anthryl chromophores in the guest.

As shown in Fig. 2b, instead of the strong Cotton effects of (*S*)-**1** at 248 nm, two opposite CD signals appeared at 243 nm and 258 nm with a crossover at 250 nm. More interestingly, a new negative peak was detected at 273 nm after a crossover at 266 nm. The new CD signal between 350 nm and 368 nm can be ascribed to the absorption of **5**. To perform an obvious and intuitive observation, 10 times magnified CD spectra of **4** ⊂ (*S*)-**1**, **4** ⊂ (*R*)-**1**, **5** ⊂ (*S*)-**1** and **5** ⊂ (*R*)-**1** between the wavelength region of the new CD signals were obtained. Similarly, completely opposite CD spectra were displayed by (*S*)-**1** with either **4** or **5** compared to (*R*)-**1**. The induced chirality expressed in the CD spectra is related to the chromophore packing model.[37] These new Cotton effects might be ascribed to the chirality transfer from the binaphthyl units to the aromatic groups lying in the cavities of (*R*)-**1** and (*S*)-**1**.[38] We can conclude that the CD signals of guests could be induced by enantiomers of chiral hosts due to the complexations of crown ether rings with the guests. The UV-vis spectra of the compounds ((*S*)-**1**, (*R*)-**1**, **4** and **5**) show typical absorption bands of binaphthyl, anthryl or pyrenyl groups. In addition, the particular absorption peaks of **4** and **5** allows the observation of chirality transfer through the CD spectra. As shown in Fig. S12a,† a positive peak at 246 nm ($\Delta\varepsilon = -53$ L mol^{-1} cm^{-1}), which is weaker than that of (*S*)-**1** with the same concentration, is presented by **2** ⊂ (*S*)-**1**, while a completely opposite CD spectrum is shown by **2** ⊂ (*R*)-**1**. The same trend was found between **3** ⊂ (*R*)-**1** and (*R*)-**1** (Fig. S12b†), and the Cotton effect value at 246 nm ($\Delta\varepsilon = -36$ L mol^{-1} cm^{-1}) is much weaker than that of **2** ⊂ (*S*)-**1**. We could find that the CD signals of the hosts were weakened at 246 nm through the assembly of the guests (**2** and **3**) with the hosts ((*R*)-**1** and (*S*)-**1**). We initially hypothesized that the hosts induced the guests to generate opposite CD signals at 246 nm.

Theoretical calculations

To learn more about the chirality transfer from the host to the guest, several meaningful quantum chemical calculations about the CD signals of [2]pseudorotaxanes (**4** ⊂ **1**) were carried out by DFT methods at the B3LYP-D3/6-31G(d,p)//SMD$_{DCM}$ level and TD-DFT methods at the TD-CAM-B3LYP-D3/6-31G(d,p)//SMD$_{DCM}$ level. Since the *R*-configuration (**4** ⊂ (*R*)-**1**) and the *S*-configuration (**4** ⊂ (*S*)-**1**) are mirror images of each other (Fig. 3), their properties are almost identical. Here we only discussed the characteristics of the *S*-configuration (**4** ⊂ (*S*)-**1**) structure to illustrate the interaction characteristics of the assembly.

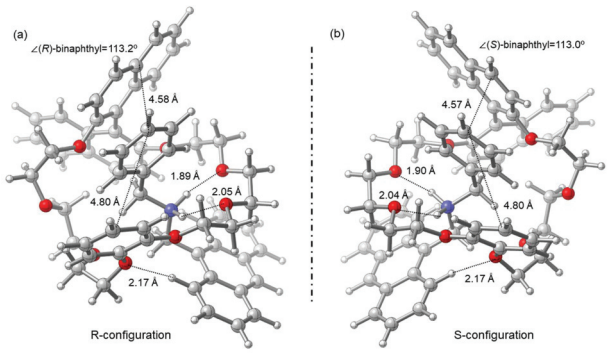

Fig. 3 The optimized structures and geometrical parameters of the (a) *R*-configuration and (b) *S*-configuration assembly **4** ⊂ **1**. Note: To save the expensive calculation cost due to the large number of atoms in the assembly, the optimization of the *R*-configuration and other calculations were performed after the calculations of the *S*-configuration were completed, and the enantiomer of the convergent *S*-configuration was optimized as the initial conformation for the *R*-configuration. Therefore, the stable conformations of the *R*-configuration and *S*-configuration are affected by the initial conformational difference, resulting in acceptable and slight calculation errors. The default optimization convergence limit of Gaussian 09 was used in all calculations, and the harmonic vibrational frequency calculations confirm that these structures have no imaginary frequencies, so that the obtained optimized structures are reliable.

As shown in Fig. 3, we found that one naphthalene ring in the binaphthalene group is substantially parallel to the benzene ring at the other end of the host crown ether (*S*)-**1** in the assembly **4** ⊂ (*S*)-**1**, and the benzene ring group of **4** is inserted in the middle to form a sandwich structure. The non-covalent interaction (NCI) analysis (Fig. 4) shows that there are some dispersion interactions between the anthracene ring of guest **4** and the binaphthalene group of host (*S*)-**1**, but the distance between them are both longer than 4.5 Å, which means there is no evident π–π interactions. In addition, the dihedral angle of the binaphthyl group changed from 112.4° to 113.0° after assembling with the guest, which is a tiny change. It means the change in the CD spectrum is not caused by the structural change of the molecular chiral chromophoric group. Moreover, the positively charged secondary ammonium of **4**

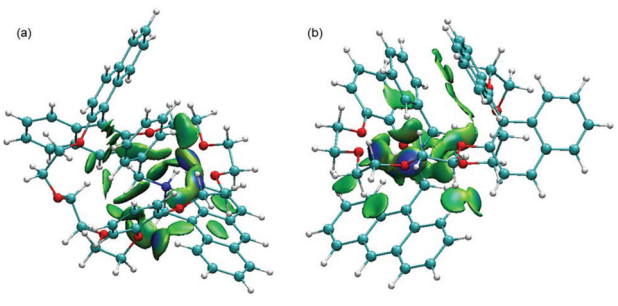

Fig. 4 The NCI analysis of the assembly **4** ⊂ (*S*)-**1**. (a and b represent two different viewing directions. The green, blue, and red regions represent the weak, strong, and repulsive interactions, respectively. Isosurface value = 0.01.)

and the electronegative oxygen of (*S*)-**1** have a significant attractive effect. It is this attractive effect that supports the stable existence of this assembly system. At the binding site, the distance between two hydrogen atoms on the secondary ammonium cation and the oxygen atom on the crown ether is 1.90 Å and 2.04 Å, which shows a certain characteristic of hydrogen bonding. At the same time, we noticed that the hydrogen atom on one side of the anthracene ring on guest **4** also has a strong attractive effect on the oxygen atom of (*S*)-**1**, and the distance between them is 2.17 Å, which also is a strong attractive CH–O interaction. The Mulliken charge distribution calculation (Table S2†) reveals that the negative charge of the oxygen atom of the crown ether (*S*)-**1** which is induced by the electrostatic field of the positive charge of guest **4**, and the positive charge of the hydrogen atom on the aromatic ring increased by the dipole–dipole induction enhanced the attractive force between the host and the guest. Meanwhile, the hydrogen atom on the other side of the same anthracene ring is close to the binaphthyl group of the host molecule but there is no oxygen atom nearby, which means the interaction between the anthracene ring of the guest and the binaphthalene group of the host is a dispersion force. Through molecular structure and NCI analyses, we can preliminarily judge that the chemical environment is different and the interaction force is not symmetrical on both sides of the guest molecule **4** in the assembly, which may be the cause of the new spectral peak in the CD spectrum of **4** ⊂ (*S*)-**1**.

To reveal the origin of the new CD signals, we calculated the theoretical CD spectra of guest **4**, host (*S*)-**1** and [2]pseudorotaxane **4** ⊂ (*S*)-**1** respectively (Table S1†). We found that the first three excited states of [2]pseudorotaxane **4** ⊂ (*S*)-**1** have the same direction, which may correspond to the triple peaks in the CD spectrum experiment. Interestingly, the symmetrical guest **4**, which should have no CD signal due to the symmetry of the C_s point group, could be optimized into an asymmetric structure without symmetry constraints to produce some weak CD signals in the calculations, and there are two opposite peaks of **4** within the range of the triple peaks of [2] pseudorotaxane **4** ⊂ (*S*)-**1**. In addition, the first singlet excited state of the independent host (*S*)-**1** is also in this range, but it shows an opposite direction to the triple peaks. As analyzed above, we found that the excitation of the triple peaks of [2] pseudorotaxane **4** ⊂ (*S*)-**1** corresponds to the first excitation of guest **4** and the first two excitations of host (*S*)-**1**. Natural transition orbital (NTO) and hole–electron distribution analyses were performed to reveal the mechanism.[39–41] According to the hole–electron distribution (Fig. 5), we found that the transitions from S_0 to S_1 or S_2 is a local excitation (LE) in anthracene for the independent guest **4**, and the transitions from S_0 to S_1 is also a LE in binaphthalene for the independent host (*S*)-**1**. The [2]pseudorotaxane **4** ⊂ (*S*)-**1** shows the same LE transition mode in anthracene or binaphthalene of the inclusion system. In addition, the NTOs show that the LE makes almost all contributions in the independent molecular system, and in the inclusion system, the LE still makes the main contributions, and the charge-transfer (CT) excitation also makes great contributions (Table S1 and Fig. S16†). To evaluate the influences of CT in the inclusion system visually, we drew the continuous hole–electron (C_{ele}–C_{hole}) distribution, which equivalently describes the hole–electron distribution with a Gaussian function,[41] and we found that there are directional shifts in the hole–electron distribution of the complexation (Fig. S17†).

Above all, we could conclude that the triple peaks in the CD spectra of the [2]pseudorotaxane originated from the LE of the host and guest molecules. And for the guest molecule in the inclusion system, the change in the chemical environment

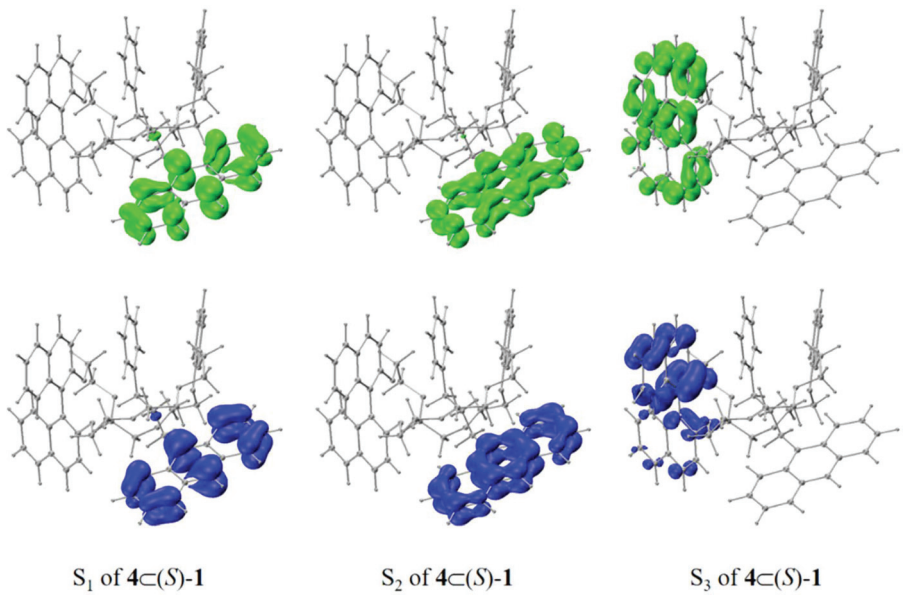

Fig. 5 Electron–hole distributions of the vertical excitations for **4** ⊂ (*S*)-**1** (green = electron, blue = hole).

destroyed the symmetry, so that new CD signals appeared in the [2]pseudorotaxane. Not only does LE provide the main contributions but CT also provides large contributions due to the assembly. As a result, the asymmetric induction between the binaphthalene of the host and the anthracene of the guest in the inclusion system allows the LE to produce a directional shift, which changes the direction and intensity of the peaks in the CD spectra. Hence the triple peaks could be observed in the CD spectrum experiment. Based on the DFT and TD-DFT calculations, we concluded that the these new CD signals were generated mainly due to the intermolecular chiral induction between anthracene and naphthalene chromophores.

FRET and K_s calculation

UV-vis spectroscopy and fluorescence spectroscopy were employed to obtain the binding constants between the hosts and the guests. As shown in Fig. 6a, there was a good spectral overlap between the emission of (*S*)-**1** (donor) and the absorption of **4** (acceptor) which is favorable for the FRET process. According to the classical description of Förster resonance energy transfer (FRET), an efficient energy transfer requires a spectral overlap between the emission of the donor and the acceptor chromophores.[42–49] Significantly, the fluorescence intensity of (*S*)-**1** at 369 nm was greatly decreased with the addition of **4** (Fig. 6b). Through a simple calculation based on the equation $\Phi_{ET} = 1 - I_{DA}/I_D$,[44] the energy-transfer efficiency (Φ_{ET}) was calculated as 75.0% in the mixed solvent ($CH_2Cl_2 : CH_3CN = 20 : 1$), measured under the conditions of [(*S*)-**1**] = [**4**] = 1.0×10^{-4} M at 367 nm with λ_{ex} = 295 nm. Similarly, the energy-transfer efficiency (Φ_{ET}) between (*R*)-**1** (donor) and **4** (acceptor) was calculated as 79.9%. Then the same experiment in the mixed solvent ($CH_2Cl_2 : CH_3CN : CH_3OH = 20 : 1 : 1$) was performed and the energy-transfer efficiency (Φ_{ET}) between (*S*)-**1** (donor) and **4** (acceptor) was calculated as 65.7% (Fig. S15†). It indicated that the inclusion strength and FRET effect between (*R*)-**1** and **4** falls off with the change in the solvent. Furthermore, the fluorescence titration experiments were carried out to investigate the binding behavior between (*R*)-**1** and **4**. As shown in Fig. S13b,† with the addition of varying quantities of **4** to the solution of (*R*)-**1**, the fluorescence emission peaks at 369 nm decreased sharply, accompanied by the appearance of enhanced triple peaks at 405 nm, 423 nm and 450 nm. The binding constant (K_s = (4.24 ± 0.24) × 10^4 M^{-1}) between (*R*)-**1** and **4** in the mixed solvent ($CH_2Cl_2 : CH_3CN$ = 20 : 1) was obtained by the nonlinear least-squares fitting method[50] (Fig. S14c†), which was consistent with the previous reports.[51–53] Using the same fluorescence titration method, the K_s value between (*R*)-**1** and **5** was calculated to be (3.55 ± 0.38) × 10^4 M^{-1} (Fig. S14d†). Furthermore, using the UV-vis absorbance titration method, the K_s value between (*R*)-**1** and **2** was calculated to be (1.28 ± 0.05) × 10^4 M^{-1} (Fig. S14a†) and the K_s value between (*R*)-**1** and **3** was calculated to be (3.17 ± 0.19) × 10^4 M^{-1} (Fig. S14b†).

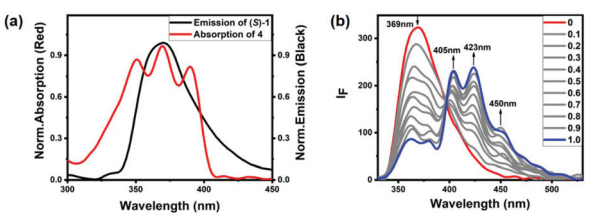

Fig. 6 (a) The normalized emission spectrum (λ_{ex} = 295 nm) of (*S*)-**1** and the absorption spectrum of **4**. (b) The fluorescence spectra (λ_{ex} = 295 nm) of (*S*)-**1** in $CH_2Cl_2 : CH_3CN$ = 20 : 1 (1.0×10^{-4} M) with different concentrations of **4**. The concentrations of **4** were 0, 1×10^{-5}, 2×10^{-5}, 3×10^{-5}, 4×10^{-5}, 5×10^{-5}, 6×10^{-5}, 7×10^{-5}, 8×10^{-5}, 9×10^{-5} and 1×10^{-4} M. The silt width was 2.5 and 2.5 nm for emission.

Conclusions

In summary, we constructed a series of [2]pseudorotaxanes by the assembly of a pair of chiral binaphthalene enantiomeric crown ethers (*R*)-**1**/(*S*)-**1** with four achiral secondary ammonium ions **2–5** containing different π-conjugated systems. CD spectroscopy studies showed that the binaphthalene groups could induce new CD signals only in the [2]pseudorotaxane structures of the host crown ethers and guest **4** with the anthryl group, indicating that a supramolecular chirality transfer process occurs from the unimolecule to [2]pseudorotaxane systems. DFT and TD-DFT calculations illustrated that this new CD signal arises mainly due to the intermolecular chiral induction between anthracene and naphthalene chromophores. By coincidence, binaphthalene and anthryl are a known effective FRET pair, so a highly efficient FRET process occurred between host **1** and guest **4**. These new observations are useful not only for globally understanding the supramolecular chirality transfer phenomena but also for designing tailored supramolecular components for versatile supramolecular chiral materials.

Experimental

Instrumentation and methods

All the reagents and solvents were commercially available and used as received without further purification. Column chromatography was performed on silica gel (200–300 mesh). NMR spectra were recorded on a Bruker AV400 instrument at 25 °C and chemical shifts were recorded in parts per million (ppm). High-resolution matrix-assisted laser desorption/ionization spectra (HR-MALDI) were measured on a Varian 7.0T FT-MS spectrometer. The UV light irradiation experiment was carried out using a ZF-7A lamp (365 nm, 8 W), and the visible light irradiation experiment (λ > 420 nm) was carried out using a CEL HXF300 xenon lamp with a cutoff filter. UV-vis spectra were recorded on a Shimadzu UV-3600 spectrophotometer equipped with a PTC-348WI temperature controller. Steady-state fluorescence emission spectra were recorded using a conventional quartz cell (lightpath 10 × 10 × 45 mm) at 25 °C on a Varian Cary

Eclipse spectrometer equipped with a Varian Cary single-cell peltier accessory to control the temperature. CD spectra were collected on a JASCO J-715 Circular Dichroism spectrometer.

Theoretical calculation

All DFT and TD-DFT calculations were performed using the Gaussian 09 software. For the stronger flexibility of the assembly, we obtained the crystal structure from ref. 54 and constructed the initial conformation by modifying it. The geometries were optimized by using the B3LYP-D3/6-31G(d,p) method for all molecules and systems.[55–57] The harmonic vibrational frequency calculations at the same level of theory were performed to reveal that the local minimum had no imaginary frequencies. The SMD solvation model with the dichloromethane solvent was used in all quantum chemistry calculations.[58] NTOs were obtained to illustrate the transition characters of all of the excited states based on the geometries of ground states using TD-DFT at the CAM-B3LYP-D3/6-31G(d,p) level.[56,59] The electron–hole distribution and NCI analyses were performed and drawn using the Multiwfn program (version 3.6) and VMD 1.9.3 tool.[60,61]

Conflicts of interest

There are no conflicts to declare.

Acknowledgements

This work was supported by the National Natural Science Foundation of China (grant no. 21772100 and 21861132001).

References

1 M. Liu, L. Zhang and T. Wang, *Chem. Rev.*, 2015, **115**, 7304–7397.
2 P. Xing and Y. Zhao, *Acc. Chem. Res.*, 2018, **51**, 2324–2334.
3 H. Cao and S. D. Feyter, *Nat. Commun.*, 2018, **9**, 3416.
4 Y. Tachibana, N. Kihara and T. Takata, *J. Am. Chem. Soc.*, 2004, **126**, 3438–3439.
5 C. Moberg, *Angew. Chem., Int. Ed.*, 1998, **37**, 248–268.
6 X. Wei, W. Wu, R. Matsushita, Z. Yan, D. Zhou, J. J. Chruma, M. Nishijima, G. Fukuhara, T. Mori, Y. Inoue and C. Yang, *J. Am. Chem. Soc.*, 2018, **140**, 3959–3974.
7 L. Pu, *Chem. Rev.*, 1998, **98**, 2405–2494.
8 H. Fenniri, B.-L. Deng and A. E. Ribbe, *J. Am. Chem. Soc.*, 2002, **124**, 11064–11072.
9 W. Shang, X. Zhu, T. Liang, C. Du, L. Hu, T. Li and M. Liu, *Angew. Chem., Int. Ed.*, 2020, **59**, 12811–12816.
10 L. Hu, K. Li, W. Shang, X. Zhu and M. Liu, *Angew. Chem.*, 2020, **59**, 4953–4958.
11 K. Ariga, T. Mori, T. Kitao and T. Uemura, *Adv. Mater.*, 2019, 1905657.
12 X. Dou, N. Mehwish, C. Zhao, J. Liu, C. Xing and C. Feng, *Acc. Chem. Res.*, 2020, **53**, 852–862.
13 X. Dou, B. Wu, J. Liu, C. Zhao, M. Qin, Z. Wang, H. Schönherr and C. Feng, *ACS Appl. Mater. Interfaces*, 2019, **11**, 38568–38577.
14 G. A. Hembury, V. V. Borovkov and Y. Inoue, *Chem. Rev.*, 2008, **108**, 1–73.
15 E. B. Kyba, K. Koga, L. R. Sousa, M. G. Siegel and D. J. Cram, *J. Am. Chem. Soc.*, 1973, **95**, 2692–2693.
16 M. Gangopadhyay, A. Maity, A. Dey, P. R. Rajamohanan, S. Ravindranathan and A. Das, *Chem. – Eur. J.*, 2017, **23**, 18303–18313.
17 H. Tanaka and S. Matile, *Chirality*, 2008, **20**, 307–312.
18 W. Zuo, Z. Huang, Y. Zhao, W. Xu, Z. Liu, X.-J. Yang, C. Jia and B. Wu, *Chem. Commun.*, 2018, **54**, 7378–7381.
19 P. Xing, Y. Li, Y. Wang, P.-Z. Li, H. Chen, S. Z. F. Phua and Y. Zhao, *Angew. Chem. Int. Ed.*, 2018, **57**, 7774–7779.
20 H.-J. Wang, H.-Y. Zhang, H. Wu, X.-Y. Dai, P.-Y. Li and Y. Liu, *Chem. Commun.*, 2019, **55**, 4499–4502.
21 J. Yao, Z. Yan, J. Ji, W. Wu, C. Yang, M. Nishijima, G. Fukuhara, T. Mori and Y. Inoue, *J. Am. Chem. Soc.*, 2014, **136**, 6916–6919.
22 A. Maity, M. Gangopadhyay, A. Basu, S. Aute, S. S. Babu and A. Das, *J. Am. Chem. Soc.*, 2016, **138**, 11113–11116.
23 K. Okano, M. Taguchi, M. Fujiki and T. Yamashita, *Angew. Chem., Int. Ed.*, 2011, **50**, 12474–12477.
24 A. A. Sobczuk, Y. Tsuchiya, T. Shiraki, S.-I. Tamaru and S. Shinkai, *Chem. – Eur. J.*, 2012, **18**, 2832–2838.
25 Y. Sang, J. Han, T. Zhao, P. Duan and M. Liu, *Adv. Mater.*, 2019, 1900110.
26 K. Nonaka, M. Yamaguchi, M. Yasui, S. Fujiwara, T. Hashimoto and T. Hayashita, *Chem. Commun.*, 2014, **50**, 10059–10061.
27 S. Sharma, M. Kataria, M. Kumar and V. Bhalla, *Angew. Chem., Int. Ed.*, 2019, **58**, 16203–16209.
28 H.-G. Fu, H.-Y. Zhang, H.-Y. Zhang and Y. Liu, *Chem. Commun.*, 2019, **55**, 13462–13465.
29 M. Gangopadhyay, A. K. Mandal, A. Maity, S. Ravindranathan, P. R. Rajamohanan and A. Das, *J. Org. Chem.*, 2016, **81**, 512–521.
30 A. K. Mandal, M. Suresh and A. Das, *Org. Biomol. Chem.*, 2011, **9**, 4811–4817.
31 J. Wu, W. Liang, T. Niu, W. Wu, D. Zhou, C. Fan, J. Ji, G. Gao, J. Men, Y. Yang and C. Yang, *Chem. Commun.*, 2018, **54**, 9206–9209.
32 C. Wang, L. Zhu, J. Xiang, Y. Yu, D. Zhang, Z. Shuai and D. Zhu, *J. Org. Chem.*, 2007, **72**, 4306–4312.
33 M. Cavazza, M. Zandomeneghi, A. Ouchi and Y. Koga, *J. Am. Chem. Soc.*, 1996, **118**, 9990–9991.
34 M. Koizumi, C. D.-B. Christiane and J.-P. Sauvage, *Eur. J. Org. Chem.*, 2004, 770–775.
35 R. Liu, Y. Zhang, W. Wu, W. Liang, Q. Huang, X. Yu, W. Xu, D. Zhou, N. Selvapalam and C. Yang, *Chin. Chem. Lett.*, 2019, **30**, 577–581.
36 H. Lai, T. Zhao, Y. Deng, C. Fan, W. Wu and C. Yang, *Chin. Chem. Lett.*, 2019, **30**, 1979–1983.
37 P. Duan, H. Cao, L. Zhang and M. Liu, *Soft Matter*, 2014, **10**, 5428–5448.

38 X.-Z. Zhu and C.-F. Chen, *Chem. – Eur. J.*, 2010, **12**, 5603–5609.
39 R. L. Martin, *J. Chem. Phys.*, 2003, **118**, 4775.
40 T. Lu and F. W. Chen, *Acta Chim. Sin.*, 2011, **69**, 2393–2406.
41 T. Lu and F. Chen, *J. Comput. Chem.*, 2012, **33**, 580–592.
42 H. Wu, Y. Chen and Y. Liu, *Adv. Mater.*, 2017, **29**, 1605271.
43 G. Liu, X. Xu, Y. Chen, X. Wu, H. Wu and Y. Liu, *Chem. Commun.*, 2016, **52**, 7966–7969.
44 J. J. Li, Y. Chen, J. Yu, N. Cheng and Y. Liu, *Adv. Mater.*, 2017, **29**, 1701905.
45 L. Giordano, T. M. Jovin, M. Irie and E. A. Jares-Erijman, *J. Am. Chem. Soc.*, 2002, **124**, 7481–7489.
46 E. Ishow, A. Credi, V. Balzani, F. Spadola and L. Mandolini, *Chem. – Eur. J.*, 1999, **5**, 984–989.
47 A. K. Mandal, M. Suresh, P. Das and A. Das, *Chem. – Eur. J.*, 2012, **18**, 3906–3917.
48 M. Suresh, A. K. Mandal, M. K. Kesharwani, N. N. Adarsh, B. Ganguly, R. K. Kanaparthi, A. Samanta and A. Das, *J. Org. Chem.*, 2011, **76**, 138–144.
49 M. Gangopadhyay, A. Maity, A. Dey and A. Das, *J. Org. Chem.*, 2016, **81**, 8977–8987.
50 Y.-X. Wang, Y.-M. Zhang and Y. Liu, *J. Am. Chem. Soc.*, 2015, **137**, 4543–4549.
51 I. Fumitaka, F. Kei-Ichiro, S. Takashi, N. Kazuko, K. Yasuhito and T. Toshikazu, *Chem. – Eur. J.*, 2011, **17**, 12067–12075.
52 A. K. Mandal, M. Gangopadhyay and A. Das, *Chem. Soc. Rev.*, 2015, **44**, 663–676.
53 A. K. Mandal, M. Suresh, M. K. Kesharwani, M. Gangopadhyay, M. Agrawal, V. P. Boricha, B. Ganguly and A. Das, *J. Org. Chem.*, 2013, **78**, 9004–9012.
54 S. J. Cantrill, M. C. T. Fyfe, A. M. Heiss, J. F. Stoddart, A. J. P. White and D. J. Williams, *Chem. Commun.*, 1999, **13**, 1251–1252.
55 A. D. Becke, *J. Chem. Phys.*, 1993, **98**, 5648–5640.
56 R. Lonsdale, J. N. Harvey and A. J. Mulholland, *J. Phys. Chem. Lett.*, 2010, **1**, 3232–3237.
57 A. K. Mandal, P. Das, P. Mahato, S. Acharya and A. Das, *J. Org. Chem.*, 2012, **77**, 6789–6800.
58 A. V. Marenich, C. J. Cramer and D. G. Truhlar, *J. Phys. Chem. B*, 2009, **113**, 6378–6396.
59 T. Yanai, D. P. Tew and N. C. Handy, *Chem. Phys. Lett.*, 2004, **393**, 51–57.
60 T. Lu and F. Chen, *J. Comput. Chem.*, 2012, **33**, 580–592.
61 W. Humphrey, A. Dalke and K. Schulten, *J. Mol. Graphics*, 1996, **14**, 33–38.